Chinese Chemical Letters 37 (2026) 111114

Contents lists available at ScienceDirect

Chinese Chemical Letters

journal homepage: www.elsevier.com/locate/cclet

Reviving the ionic conductivity of air-instable solid-state electrolytes *via* a facile heat treatment

Liang Ming[a,b,1], Miao Deng[a,b,1], Siwu Li[c,*], Ziling Jiang[a,b], Lin Li[a,b], Ziyu Lu[a,b], Qiyue Luo[a,b], Jie Yang[a,b], Zhonghui Cui[d,*], Chuang Yu[a,b,*]

[a] School of Chemistry and Chemical Engineering, Huazhong University of Science and Technology, Wuhan 430074, China
[b] State Key Laboratory of Advanced Electromagnetic Engineering and Technology, School of Electrical and Electronic Engineering, Huazhong University of Science and Technology, Wuhan 430074, China
[c] Academy of Advanced Interdisciplinary Research, Xidian University, Xi'an 710071, China
[d] Zhejiang Intelligent Transportation Technology Innovation Center, Ningbo 315000, China

ARTICLE INFO

Article history:
Received 21 December 2024
Revised 13 March 2025
Accepted 18 March 2025
Available online 18 March 2025

Keywords:
All-solid-state lithium batteries
Sulfide electrolyte
Halide electrolyte
Ionic conductivity
Air stability

ABSTRACT

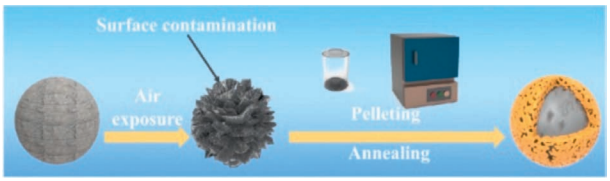
The quest for sustainable and efficient energy storage solutions has led to significant advancements in the field of solid-state batteries, with a particular focus on solid-state electrolytes (SSEs) especially highly ionic conductive sulfide and halide materials. However, the air instability of these SSEs not only limits their mass production but also poses environmental and safety risks. Herein, the damage of humid-air exposure on the structure and electrochemical properties of $Li_{5.5}PS_{4.5}Cl_{0.8}Br_{0.7}$ and Li_3InCl_6 is evaluated, and a subsequent heat treatment is proposed and proven effective to recover the damage, whose mechanisms are pinpointed through XRD data with Retvield refinement. For the exposed samples, a lattice contraction occurs as the hydrolysis reaction caused by H_2O from humid air severely damages the structure, which impedes lithium-ion transport. After heat treatment, a lattice rearrangement can rebuild sufficient lithium-ion pathway in the material, leading to the greatly improved ionic conductivity. As a result, the treated electrolytes provide greatly promoted ionic conductivity (from 0.95 mS/cm to 1.8 mS/cm for Li_3InCl_6, from 1.24 S/cm to 7.04 S/cm for $Li_{5.5}PS_{4.5}Cl_{0.8}Br_{0.7}$). More importantly, ASSBs employed with the treated electrolytes achieve outstanding long-term cycling and rate performance, even guarantee considerable capacity output of ~217 and ~159 mAh/g under extreme conditions of 60 and –20 °C, illustrating significantly improved electrochemical reaction kinetics and the impressive reliability of the heat treatment method.

© 2026 Published by Elsevier B.V. on behalf of Chinese Chemical Society and Institute of Materia Medica, Chinese Academy of Medical Sciences.

Lithium-ion batteries (LIBs) have made large revolution in the 3C electronic devices and electric vehicles market due to their diverse energy storage characteristics [1,2]. However, conventional LIBs are criticized by the inherent flammability of organic liquid electrolyte and energy limit of commercial electrode materials [3,4]. In this regard, replacing commonly-used liquid electrolytes with solid electrolytes to construct all-solid-state batteries (ASSBs) is promising to address both the safety and energy density issues in developing next-generation LIBs [5–7]. With significant progress in recent years, sulfide-, halide- and oxide-based solid-state electrolytes (SSEs) have been developed for next-generation ASSBs [8–11]. Notably, sulfide electrolytes such as chloride-rich argyrodite delivers ultrahigh ionic conductivity, reaching the level of liquid electrolytes [12–15]. However, one of the main hurdles is the hydrolysis reaction at the interface, as it is intrinsically instable in ambient humidity, leading to the release of toxic H_2S and thereby a tremendous decrease in the ionic conductivity [16]. Unfortunately, similar situations exist in halide solid electrolytes [17–19]. Halide SSEs have also gained wide attention recently due to their simple synthesis, relatively high ionic conductivity, good oxidative stability with high-voltage electrodes, and soft texture for cold-press procedure in battery assembly [10,20–22]. Nevertheless, the poor humid-air stability largely increases their cost in application due to the whole synthesis and subsequent storage procedures conducted in argon atmosphere [23]. Therefore, it is worthwhile to develop effective approaches in promoting the air-stability or lowering the processing complexity of SSEs without sacrificing their electrochemical performance especially ionic conductivity.

* Corresponding authors.
E-mail addresses: lisiwu@xidian.edu.cn (S. Li), zhonghui.cui@gmail.com (Z. Cui), cyu2020@hust.edu.cn (C. Yu).
[1] These authors contributed equally to this work.

https://doi.org/10.1016/j.cclet.2025.111114
1001-8417/© 2026 Published by Elsevier B.V. on behalf of Chinese Chemical Society and Institute of Materia Medica, Chinese Academy of Medical Sciences.



Scheme 1. Schematic illustration of the degradation of solid electrolytes after air exposure (humidity of 30%) and corresponding heat treatment.

To address these air stability issues, researchers have developed a variety of strategies. One approach involves the modification of the SSEs' structures through chemical or physical interactions to enhance their resistance to air and moisture [24]. Another strategy includes the development of new materials with improved air stability, such as hybrid electrolytes that combine the benefits of sulfide and halide SSEs [25–27]. Additionally, surface modifications or elemental doping of electrolytes have been explored to mitigate interface reactions and improve the compatibility between SSEs and humid air [28–32]. The use of protective coatings and the creation of interfacial passivation layers have also been employed to prevent direct contact between the SSEs and the atmosphere, thereby enhancing the overall stability and performance of the batteries [33–35]. In general, these strategies have been proven effective on promoting the air stability of SSEs to some extent, but their procedures are relatively complex or time/resource consuming with high cost, and most of them do harm to the electrochemical performance of the electrolyte especially ionic conductivity. What is more, up till now, there still lacks systematic studies on the degradation mechanism of these SSEs upon air exposure, which impedes the development of ASSBs.

In this work, we identify the structural and electrochemical changes of both sulfide and halide SSEs after air exposure (with the relative humidity of open air controlled to approximately 30%). Thereafter, a subsequent annealing process at relatively low temperatures (~300 °C for halide and ~500 °C for sulfide) under vacuum was applied to the exposed SSEs, and for the first time, we discovered the phenomenon of recovery on their electrochemical/structural properties (Scheme 1). Our work seeks to investigate (1) the degradation mechanism of prepared sulfide and halide SSEs during air exposure and (2) chemical reactions occurring during the recovery process. Specifically, halide electrolyte Li_3InCl_6 and sulfide electrolyte $Li_{5.5}PS_{4.5}Cl_{0.8}Br_{0.7}$ were chosen as examples in our study for their high ionic conductivity before air exposure. Moreover, a prominent recovery of structure and electrochemical properties was achieved in the exposed electrolytes since the hydrates formed after moisture exposure can be excluded *via* a facile post-heating. More significantly, the reheated electrolytes can be successfully applied in ASSBs with high initial discharge capacities and outstanding cycling stability at high current rates, and considerable capacity output under high (60 °C) and low (−20 °C) temperatures was performed as well.

First, the behavior of SSEs after air exposure was studied. For instance, $Li_{5.5}PS_{4.5}Cl_{0.8}Br_{0.7}$ was first synthesized through ball-milling method with a subsequent calcination. Thereafter, the as-synthesized powder was pressed into a pellet with a diameter of 10 mm, as shown in Fig. 1. After an air exposure (relative humidity of 30%) for 30 min, it can be clearly observed that the color of $Li_{5.5}PS_{4.5}Cl_{0.8}Br_{0.7}$ pellets changed from light grey to dark grey or even black, suggesting the occurrence of significant chemical reactions. Interestingly, however, when the pellets were subjected to a heat treatment under argon atmosphere at different temperatures including 350, 400, 450 and 500 °C, their color transformed again into different states, which are all lighter than the exposed one. With higher the temperature applied, the lighter the color becomes. The pellet treated at 500 °C even changed to a white appearance.

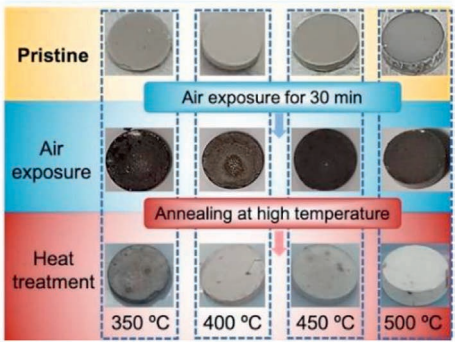


Fig. 1. Digital photos of $Li_{5.5}PS_{4.5}Cl_{0.8}Br_{0.7}$ SSE pellets at different states and after heat treatment under different temperatures.

To investigate the effect of this reheating treatment on other SSEs, we took halide electrolyte Li_3InCl_6 as an example (Fig. S1 in Supporting information). Different from the $Li_{5.5}PS_{4.5}Cl_{0.8}Br_{0.7}$ SSE pellets, after air exposure for 10 min, the pellets of Li_3InCl_6 stayed amost unchanged. When a reheating treatment under various temperatures was applied, these pellets well retained their shape with slight difference on the color. At 200 °C, the pellet is in a white color. At 300 °C, the pellet becomes light grey, which is almost the same as the pristine state. As the temperature increases, the color became slightly darker, which was converse to the phenomenon on $Li_{5.5}PS_{4.5}Cl_{0.8}Br_{0.7}$. We also conducted the same experiment on Li_3InCl_6 in a powder form with longer exposure time. As shown in Fig. S2 (Supporting information), after an exposure time of 30 min and a heat treatment at 300 °C, the Li_3InCl_6 powder well maintained its white color, and its pellet kept a grey feature throughout the procedure.

To further evaluate the effect of our heat treatment on the above electrolytes, electrochemical tests were employed. Fig. 2a shows the ionic conductivity of the Li_3InCl_6 pellets under different states. Clearly, after air exposure, the ionic conductivity of the pellet drops from the pristine value of 1.87 mS/cm to 0.95 mS/cm, which means a considerable damage to the electrolyte's electrochemical function. Upon heat treatment at 200 °C, however, the pellet experienced a remarkable increase on the ionic conductiv-

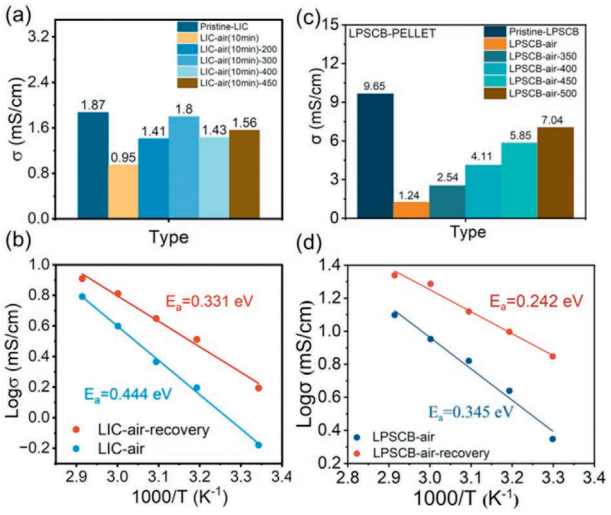


Fig. 2. Room-temperature ionic conductivity of (a) Li_3InCl_6 and (c) $Li_{5.5}PS_{4.5}Cl_{0.8}Br_{0.7}$ pellets at different states. Activation energy of (b) Li_3InCl_6 and (d) $Li_{5.5}PS_{4.5}Cl_{0.8}Br_{0.7}$.

ity to 1.41 mS/cm. When the temperature rise to 300 °C, the pellet nearly revived its pristine state, showing an ionic conductivity of 1.80 mS/cm. We further tested the pellets' ionic conductivity after treatment under higher temperatures including 400 and 450 °C, though the values could not exceed that at 300 °C, they are still at a relatively high level. The pellet was also exposed for 30 min and treated under 300 °C. As shown in Fig. S4a (Supporting information), both the pellet and powder sample confront a dramatic decrease of ionic conductivity after 30 min's air exposure, but those values surge after the treatment (from 0.66 mS/cm to 1.56 mS/cm, and 0.13 mS/cm to 0.98 mS/cm, respectively). To investigate whether air exposure causes damage to SSEs, and because the pellet sample offers better consistency in experimental conditions (due to a more uniform air contact area) compared to the powder sample, we selected the LIC pellet sample exposed to air for 30 min for subsequent characterization and testing, denoted as LIC-air.

The activation energy of the pellet was also analyzed (Fig. 2b), which depicts that the SSE after heat treatment (at 300 °C, denoted as LIC-air-300) exhibits an accelerated electrochemical kinetics by the reduced activation energy value (from 0.444 eV to 0.331 eV). Thereafter, the same testing procedure was conducted on $Li_{5.5}PS_{4.5}Cl_{0.8}Br_{0.7}$ SSE. Identically, the sulfide electrolyte experienced a similar trend: After air-exposure the ionic conductivity of the material drops from 9.65 mS/cm to 1.24 mS/cm, and the value rises after heat treatment. Under 500 °C, impressively, the electrolyte regains an ionic conductivity of 7.04 mS/cm (Fig. 2c). Furthermore, the powder LPSCB samples suffer sharp reduction to 0.81 mS/cm after 30 min's air exposure, but restore to 2.41 mS/cm after following annealing process (Fig. S4b in Supporting information) [36–38]. As shown in Fig. 2d, the activation energy of the $Li_{5.5}PS_{4.5}Cl_{0.8}Br_{0.7}$ SSE also reduced significantly after the heat treatment (from 0.345 eV to 0.242 eV). These results preliminarily demonstrate the effectiveness of the reheat strategy on addressing the air stability issues of SSEs. The influence of air and post-heat treatment on the morphology was clarified. Fig. S3 (Supporting information) displays the scanning electron microscopy (SEM) images of pristine Li_3InCl_6, $Li_{5.5}PS_{4.5}Cl_{0.8}Br_{0.7}$. Additionally, the SEM images show that the particles are evenly distributed across the surface, with uniform size and no clustering or irregular aggregation.

X-ray diffraction (XRD) was then applied to reveal the structural evolution of the above SSEs under different states. For $Li_{5.5}PS_{4.5}Cl_{0.8}Br_{0.7}$, after exposure to air for 30 min (named as LPSCB-air), the sample suffers from profound weakening of peak intensity at 15.3°, 17.7°, 25.2°, 29.7°, 31.1°, 44.6°, 47.5° and 52.1°, corresponding to the degradation of cubic argyrodite structure (PDF #34–0688) with an F-43 m space group (Fig. S5 in Supporting information) [39]. After the heat treatment at 350, 400, 450, 500 °C (denoted as LPSCB-air-recovery), the peak intensity of the argyrodite signals rerise, illustrating the partial structural recovery of the sulfide electrolyte through subsequent heating. Besides, there emerges several extra signals of Li_3PO_4 phase (PDF #15–0760) at 29.0°, 33.5° and 48.4°, disclosing the formation of crystalline impurities upon sintering due to the participance of by-products from H_2O adsorption during air exposure. For Li_3InCl_6, the XRD patterns demonstrate a slight weakening of peak intensity after air-exposure (LIC-air), and a recovery can also be observed through heating at different temperatures (Fig. S6 in Supporting information). Heating at 300 °C restores the peak intensity more effectively than at 200 °C. However, at 400 °C, an impurity peak corresponding to $InCl_3$ appears at 11.106°, which could potentially impact the ionic conductivity of the electrolyte. Notably, LPSCB-air-500 exhibits a well-defined crystalline phase, indicating that the argyrodite structure has been effectively restored. At the same time, the Li_3PO_4 signals are relatively prominent. For Li_3InCl_6, the XRD patterns demonstrate a slight weakening of peak intensity after air-exposure (LIC-air), and a recovery can also be observed through heating at 300 °C (LIC-air-300, Fig. S6). All the sample data were then processed with Rietveld refinement to further track the structure evolution in an atomic level. As shown in Figs. 3a–c and Tables S1–S3 (Supporting information), the lattice parameter α of LIC-air shows marked decrease compared to that of LIC-Pristine (from 6.408511 Å to 6.406925 Å), which can be ascribed to the local lattice collapse caused by the H_2O adsorption and hydrolysis [40,41]. In comparison, the lattice parameter α increased to 6.40719 Å, which is attributed to the removal of H_2O and lattice rearrangement in the LIC structure. Similar to the XRD results, the XPS spectra of the Li_3InCl_6 electrolytes at pristine, air-exposed and heat-treated samples (Fig. S7 in Supporting information) are essentially identical, with the In $3d_{5/2}$ peak at 445.8 eV and In $3d_{3/2}$ peak at 453.3 eV, resembling the reported values for In^{3+}-Cl^- species [14,28]. This recovery of sufficient lattice volume contributes to the promoted ionic conductivity of LIC-air-300 [42]. As for $Li_{5.5}PS_{4.5}Cl_{0.8}Br_{0.7}$, however, an expansion of lattice parameters can be observed after air exposure, which can be due to

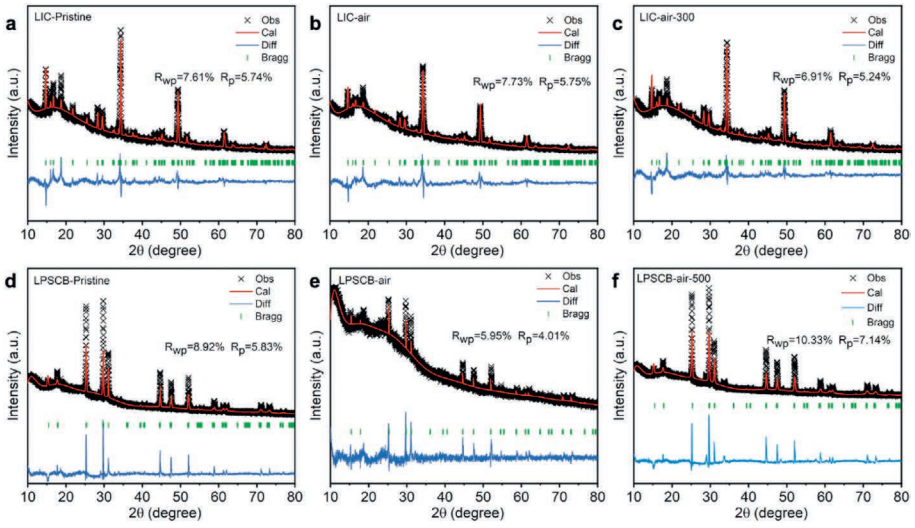


Fig. 3. XRD patterns and Retvield refinement of (a) LIC-Pristine, (b) LIC-air, (c) LIC-air-300, (d) LPSCB-Pristine, (e) LPSCB-air and (f) LPSCB-air-500.

the formation of massive surface impurities (Figs. 3d and e, Tables S4–S6 in Supporting information) [43]. After heat treatment, though Li_3PO_4 is formed in LPSCB-air-recovery, part of the impurities are excluded with a partial recovery of lattice volume, which finally boosts the lithium ion transport in the electrolyte (Fig. 3f). Fig. S8 (Supporting information) presents the P 2p region spectra of $Li_{5.5}PS_{4.5}Cl_{0.8}Br_{0.7}$ electrolytes. LPSCB-pristine exhibits a P 2p signal at 132.0 eV. In the case of LPSCB-air, oxysulfides (PO_xS_y) at 133.0 eV form after exposure, resulting from the oxidation of S^{2-} during the air exposure. And the intensity also increases after 500 °C heat treatment. Furthermore, P-O signal can also be observed at 133.6 eV in the LPSCB-air-500, indicating the formation of Li_3PO_4 and confirming the above XRD results [44,45].

To evaluate the electrochemical performance of pristine LIC and LPSCB, SSBs using the pristine electrolytes and ZrO_2@$LiNi_{0.9}Co_{0.05}Mn_{0.05}O_2$ were constructed and cycled in the voltage range of 2.4–3.7 V (*vs.* Li-In) at room temperature. As depicted in Fig. S10 (Supporting information), the LPSCB-pristine and LIC-pristine cells deliver excellent cyclability at 0.5 and 2.0 C, respectively. For the long-term cycling performance, the SSBs using LPSCB-pristine shows high discharge capacities and capacity retention of 93.0% during 200 cycles. Furthermore, LIC-pristine shows the initial discharge capacity of 170.3 mAh/g at 2.0 C after 200 cycles (capacity retention of 97.1%). Based on the results, LPSCB-pristine and LIC-pristine exhibit excellent stability towards ZrO_2@$LiNi_{0.9}Co_{0.05}Mn_{0.05}O_2$.

The electrochemical performance of the prepared electrolytes was then assessed by assembling ASSBs with ZrO_2-coated $LiNi_{0.9}Mn_{0.05}Co_{0.05}O_2$ as the cathode and Li-In alloy as the anode. $Li_{5.5}PS_{4.5}Cl_{0.8}Br_{0.7}$ was first utilized as the electrolyte in full cell preparation, with the cell comprising the pristine sample named pristine LPSCB, exposed sample named as LPSCB-air, and the reheated one named as LPSCB-air-500. In long-term cycling performance test (Fig. 4a and Fig. S9 in Supporting information), the cells were allowed to charge and discharge at 0.2 C for the first cycle, and then tested under 0.5 C. Notably, the LPSCB-air-500 cell delivers an initial discharge capacity of 210 and 203 mAh/g at 0.2 and 0.5 C, respectively, and well retain its capacity output after 200 cycles (capacity retention of 71.0%). In comparison, the LPSCB-air cell gives a lower initial capacity of 196 and 181 mAh/g, and only retains 37.0% of the initial capacity after 200 cycles. Accordingly, the cycling data were used to calculate the d*Q*/d*V* curves (Figs. 4b and c). Obviously, the LPSCB-air cell exhibits dramatic peak position shifts (a negative shift on the anodic branches and positive shift on the cathodic branches), and all the peaks show evident reduction of intensity upon cycling. However, this phenomenon becomes negligible on the LPSCB-air-500 cell, which suggests that the severe loss of Li inventory (related to the decay of H2-H3 phase transition) and decrease of Li-ion conduction pathways in the cell is effectively suppressed in the LPSCB-air-500 cell [36–38]. Similarly, the discharge capacities of the ASSBs based on exposed and retreated Li_3InCl_6 (denoted as LIC-air and LIC-air-300 cell, respectively) demonstrate notable discrepancy, with the former giving only 201 mAh/g and the latter giving 142 mAh/g at 0.2 C, respectively (Fig. S10). Additionally, the cycling data were used to calculate the d*Q*/d*V* curves (Figs. S10b and c). For the LIC-air cell, an irreversible H2-H3 phase transition is more pronounced during the charging process. However, this phenomenon is almost absent in the LIC-air-300 cell, which may explain why the LIC-air-300 battery exhibits a higher initial capacity. The advantage can also be achieved in other extreme test conditions: (1) At a current rate of 2.0 C, the cell is able to provide an initial discharge capacity of 167 mAh/g and retention of 70.0% after 900 cycles (Fig. 4d); (2) Under 60 °C and −20 °C, the cell still maintains an average capacity as high as ~217 (0.5 C) and ~159 mAh/g (0.1C), respectively (Figs. S11 and S12 in Supporting information). Rate performance of the ASSBs with the above electrolytes were further tested. As shown in Fig. 4e, the LPSCB-air cell shows an average discharge capacity of ~205 mAh/g at 0.1 C, but the value declines to only ~133 mAh/g at 1.0 C, and even to ~13 mAh/g at 5 C, showing poor electrochemical kinetics. In sharp contrast, the LPSCB-air-500 cell delivers an average capacity of 224, 188 and 115 mAh/g at 0.1, 1.0 and 5.0 C, respectively, and the values can be well recovered when the current rates are switched back. For the LIC-air and LIC-air-300 cell, this

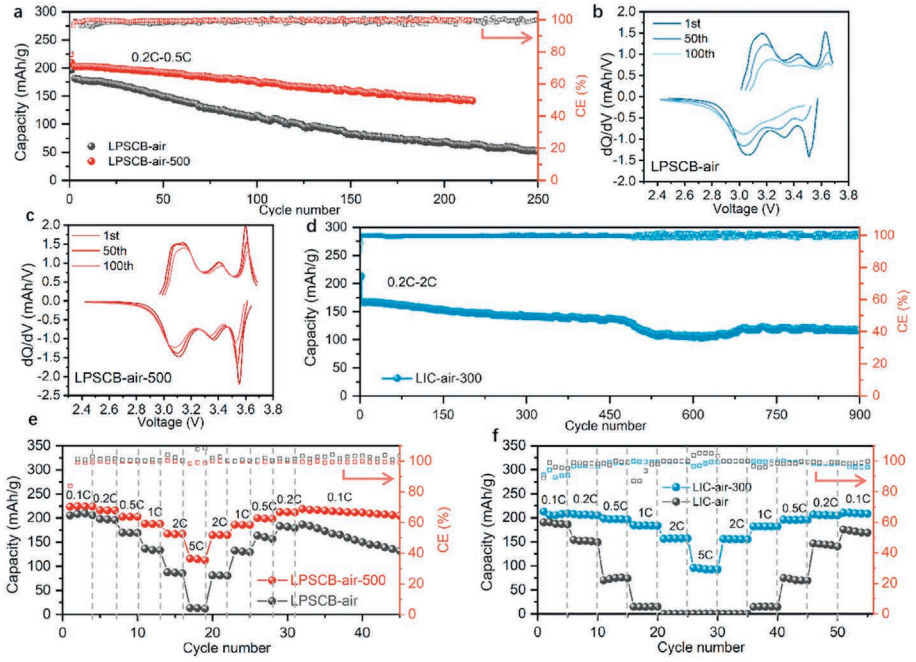


Fig. 4. Long-term cycling performance of ASSBs with (a) Li_3InCl_6 and (b) $Li_{5.5}PS_{4.5}Cl_{0.8}Br_{0.7}$ electrolytes before and after reheating treatment. The d*Q*/d*V* curves of ASSBs at various cycle numbers with $Li_{5.5}PS_{4.5}Cl_{0.8}Br_{0.7}$ electrolytes (c) before and (d) after reheating treatment. Rate performance of ASSBs with (e) Li_3InCl_6 and (f) $Li_{5.5}PS_{4.5}Cl_{0.8}Br_{0.7}$ electrolytes before and after reheating treatment.

disparity further enlarged: (1) In rate test (Fig. 4f), the LIC-air cell delivers only 206, 197 and 184 at 0.2, 0.5 and 1.0 C, respectively, which is 73.0%, 38.0% and 7.8% to that of the LIC-air-300 cell; at 2.0 and 5.0 C, the LIC-air cell is incapable to release any capacity, while those of the LIC-air-300 cell well retain at 157 and 93 mAh/g, respectively; (3) the voltage hysteresis (calculated by the difference between the median voltage of charge and discharge) of the LIC-air-300 cell is 30, 78 and 147 mV at 0.2, 0.5 and 1.0 C, respectively (Fig. S13a in Supporting information), much smaller than those of the LIC-air cell under corresponding rates (339, 691 and 1034 mV at 0.2, 0.5 and 1.0 C, respectively, Fig. S13b in Supporting information). Therefore, it can be concluded that the degradation of both halide and sulfide electrolytes leads to a serious loss of electrochemical kinetics and lithium inventory during battery cycling, and a restored crystal structure by facile heat treatment is capable of saving the electrolyte in battery performance, showing great potential in practical application.

In summary, we have disclosed the significant damage of humid-air exposure on the structure and electrochemical properties of air-instable SSEs including $Li_{5.5}PS_{4.5}Cl_{0.8}Br_{0.7}$ and Li_3InCl_6, and a subsequent heat treatment was proposed and proven effective to recover the damage, whose mechanisms were pinpointed through XRD data with Retvield refinement. Specifically, the contraction of lattice volume of the electrolytes caused by the hydrolysis reaction from humid air is the culprit to the electrolytes' degradation. After proper heat treatment, a lattice rearrangement occurs and rebuilds sufficient lithium-ion pathway in the material. Consequently, the treated electrolytes provided greatly promoted ionic conductivity from 0.95 mS/cm to 1.8 mS/cm for Li_3InCl_6, from 1.24 mS/cm to 7.04 mS/cm for $Li_{5.5}PS_{4.5}Cl_{0.8}Br_{0.7}$. More importantly, the ASSBs employed with the treated electrolytes achieved outstanding long-term cycling and rate performance, even guaranteed considerable capacity output of ~217 and ~159 mAh/g under extreme conditions of 60 and –20 °C, illustrating significantly improved electrochemical reaction kinetics and the impressive reliability of the heat treatment method. While the results and achievements presented here are preliminary, they have opened a brand-new perspective for promoting the chemical stability and thereof the industrialization of air-instable SSEs. To further understand the role of heat treatment on the evolution of SSEs and boost their development, comprehensive studies gathering a series of *ex-situ* and *in-situ* spectroscopic technologies and theoretical calculations are underway in our lab, which will also offer useful knowledge that enables the advent of high-performance and low-cost ASSBs.

Declaration of competing interest

The authors declare that they have no known competing financial interests or personal relationships that could have appeared to influence the work reported in this paper.

CRediT authorship contribution statement

Liang Ming: Writing – original draft, Software, Methodology, Investigation, Formal analysis, Data curation, Conceptualization. **Miao Deng:** Writing – original draft, Methodology, Investigation, Formal analysis, Data curation, Conceptualization. **Siwu Li:** Writing – original draft, Supervision, Software, Resources, Methodology, Investigation, Formal analysis, Data curation, Conceptualization. **Ziling Jiang:** Methodology, Investigation, Formal analysis, Data curation, Conceptualization. **Lin Li:** Methodology, Investigation, Formal analysis, Data curation, Conceptualization. **Ziyu Lu:** Investigation, Formal analysis, Data curation, Conceptualization. **Qiyue Luo:** Investigation, Formal analysis, Data curation, Conceptualization. **Jie Yang:** Investigation, Formal analysis, Data curation, Conceptualization. **Zhonghui Cui:** Writing – original draft, Supervision, Resources, Project administration, Funding acquisition, Conceptualization. **Chuang Yu:** Writing – original draft, Supervision, Software, Resources, Methodology, Investigation, Formal analysis, Data curation, Conceptualization.

Acknowledgments

This work was supported by relevant National programmes of China. It was also supported by the National Key Research and Development Program (No. 2021YFB2500200). This work is also supported by the National Natural Science Foundation of China (No. 52177214), the Postdoctoral Science Research Program of Shaanxi (No. 30102230001) and the Postdoctoral Fellowship Program of CPSF (No. GZB20230558). We gratefully acknowledge the Analytical and Testing Center of HUST, Instrumental Analysis Center of Xidian University and Comprehensive Experimental Center for Chemistry and Bioscience in Xidian University allow us to use the facilities.

Supplementary materials

Supplementary material associated with this article can be found, in the online version, at doi:10.1016/j.cclet.2025.111114.

References

[1] Y. Ding, Z.P. Cano, A. Yu, J. Lu, Z. Chen, Electrochem. Energy Rev. 2 (2019) 1–28.
[2] M. Li, J. Lu, Z. Chen, K. Amine, Adv. Mater. 30 (2018) 1800561.
[3] Y. Chen, Y. Kang, Y. Zhao, et al., J. Energy Chem. 59 (2021) 83–99.
[4] J. Duan, X. Tang, H. Dai, et al., Electrochem. Energy Rev. 3 (2019) 1–42.
[5] Y.S. Meng, V. Srinivasan, K. Xu, Science 378 (2022) eabq3750.
[6] Q. Zhao, S. Stalin, C.Z. Zhao, L.A. Archer, Nat. Rev. Mater. 5 (2020) 229–252.
[7] H. Zhu, S. Li, L. Peng, et al., Nano Energy 125 (2024) 109571.
[8] C. Yu, L. van Eijck, S. Ganapathy, M. Wagemaker, Electrochim. Acta 215 (2016) 93–99.
[9] T. Asano, A. Sakai, S. Ouchi, et al., Adv. Mater. 30 (2018) 1803075.
[10] X. Li, J. Liang, N. Chen, et al., Angew. Chem. Int. Ed. 58 (2019) 16427–16432.
[11] C. Wang, K. Fu, S.P. Kammampata, et al., Chem. Rev. 120 (2020) 4257–4300.
[12] C. Yu, S. Ganapathy, J. Hageman, L. van Eijck, et al., ACS Appl. Mater. Interfaces 10 (2018) 33296–33306.
[13] S. Chen, C. Yu, C. Wei, et al., Energy Mater. Adv. 4 (2023) 0019.
[14] Q. Guo, F. Xu, L. Shen, et al., Energy Mate. Adv. 2022 (2022) 9753506.
[15] R. Guo, K. Zhang, W. Zhao, et al., Energy Mater. Adv. 4 (2023) 0022.
[16] F. Zhao, J. Liang, C. Yu, et al., Adv. Energy Mater. 10 (2020) 1903422.
[17] J. Liang, X. Li, C. Wang, et al., Energy Mater. Adv. 4 (2023) 0021.
[18] Q. Luo, L. Ming, D. Zhang, et al., Energy Mater. Adv. 4 (2023) 0065.
[19] M.K. Tufail, P. Zhai, M. Jia, N. Zhao, X. Guo, Energy Mater. Adv. 4 (2023) 0015.
[20] X.K. Liu, Y.X. Zhou, F.H. Mi, X.L. Ma, C.W. Sun, Energy Storage Mater. 72 (2024) 103737.
[21] K. Tuo, C. Sun, S. Liu, Electrochem. Energy Rev. 6 (2023) 17.
[22] K. Tuo, C. Sun, C.A. López, M.T. Fernández-Díaz, J.A. Alonso, J. Mater. Chem. A 11 (2023) 15651–15662.
[23] X. Li, J. Liang, J. Luo, et al., Energy Environ. Sci. 12 (2019) 2665–2671.
[24] Y. Cai, C. Li, Z. Zhao, D. Mu, B. Wu, ChemElectroChem 9 (2022) 2101479.
[25] F. Liu, L. Gao, Z. Zhang, et al., Energy Storage Mater 64 (2024) 103072.
[26] K. Tuo, F. Yin, C. Sun, ACS Sustain Chem. Engin. 12 (2024) 7012–7025.
[27] D. Yang, J. Li, C. Liu, W. Xing, J. Zhu, J. Energy Chem. 82 (2023) 122–138.
[28] Z.Q. Wang, Z.Y. Xiong, X.J. Ma, et al., Org. Electron. 44 (2017) 110–114.
[29] Z. Jiang, Y. Xiao, L. Li, et al., ChemSusChem 18 (2025) e202401664.
[30] Y. Sun, K. Suzuki, K. Hara, et al., J. Power Sources 324 (2016) 798–803.
[31] T. Ohtomo, A. Hayashi, M. Tatsumisago, K. Kawamoto, J. Solid State Electrochem. 17 (2013) 2551–2557.
[32] G. Liu, D. Xie, X. Wang, et al., Energy Storage Mater. 17 (2019) 266–274.
[33] J. Liang, X. Li, Y. Zhao, et al., Adv. Energy Mater. 9 (2019) 1902125.
[34] W.D. Jung, M. Jeon, S.S. Shin, et al., ACS Omega 5 (2020) 26015–26022.
[35] K.H. Park, D.Y. Oh, Y.E. Choi, et al., Adv. Mater. 28 (2016) 1874–1883.
[36] L. Li, J. Yao, R. Xu, et al., Energy Storage Mater. 63 (2023) 103016.
[37] R. Song, J. Yao, R. Xu, et al., Adv. Energy Mater. 13 (2023) 2203631.
[38] H. Yan, J. Yao, Z. Ye, et al., Chin. Chem. Lett. 36 (2025) 109568.
[39] C. Yu, S. Ganapathy, N.J. de Klerk, et al., J. Am. Chem. Soc. 138 (2016) 11192–11201.
[40] W. Li, J. Liang, M. Li, et al., Chem. Mater. 32 (2020) 7019–7027.
[41] Y. Ni, C. Huang, H. Liu, Y. Liang, L.Z. Fan, Adv. Funct. Mater. 32 (2022) 2205998.
[42] A. Mills, S. Kalnaus, W.Y. Tsai, et al., ACS Energy Lett. 9 (2024) 2677–2684.
[43] L. Li, Z. Jiang, J. Yang, et al., Adv. Funct. Mater. 35 (2025) 2410008.
[44] Y.T. Chen, M.A.T. Marple, D.H.S. Tan, et al., J. Mater. Chem. A 10 (2022) 7155–7164.
[45] Y. Nikodimos, C.J. Huang, B.W. Taklu, W.N. Su, B.J. Hwang, Energy Environ. Sci. 15 (2022) 991–1033.